Improving the light stability of perovskite solar cell with new hole transport material based on spiro[fluorene-9,9′-xanthene]

Huiming Luo[1,2†], Zheng Zhang[1†], Ligang Yuan[1], Jiarong Wang[1], Bin Li[3], Sijing Wang[3], Mojtaba Abdi-Jalebi[2], Lei Shi[4], Wenjun Zhang[4], Kunpeng Guo[3*], Liming Ding[5] and Keyou Yan[1*]

Abstract

Development of suitable hole transport materials is vital for perovskite solar cells (PSCs) to diminish the energy barrier and minimize the potential loss. Here, a low-cost hole transport molecule named SFX-POCCF3 (23.72 $/g) is designed with a spiro[fluorene-9,9′-xanthene] (SFX) core and terminated by trifluoroethoxy units. Benefiting from the suitable energy level, high hole mobility, and better charge extraction and transport, the PSCs based on SFX-POCCF3 exhibit improved open-circuit voltage by 0.02 V, therefore, the PSC device based on SFX-POCCF3 exhibits a champion PCE of 21.48%, which is comparable with the control device of Spiro-OMeTAD (21.39%). More importantly, the SFX-POCCF3 based PSC possesses outstanding light stability, which retains 95% of the initial efficiency after about 1,000 h continuous light soaking, which is in accordance with the result continuous output at maximum power point. Whereas, Spiro-OMeTAD witnesses a rapid decrease to 80% of its original efficiency after 100 h light soaking. This work demonstrated that an efficient alignment of energy levels between HTL and perovskite will lead to significant highly efficient PSCs with remarkably enhanced light stability.

Keywords Hole transport materials, Perovskite solar cell, Deeper HOMO level, Low cost

†Huiming Luo and Zheng Zhang contributed equally to this work.

*Correspondence:
Kunpeng Guo
guokunpeng@tyut.edu.cn
Keyou Yan
kyyan@scut.edu.cn
[1] School of Environment and Energy, Guangdong Provincial Key Laboratory of Solid Wastes Pollution Control and Recycling, South China University of Technology, Guangzhou 510000, China
[2] Institute for Materials Discovery, University College London, Malet Place, London WC1E 7JE, UK
[3] Ministry of Education Key Laboratory of Interface Science and Engineering in Advanced Materials, Taiyuan University of Technology, Taiyuan 030024, Shanxi, China
[4] Hangzhou Zhongneng Photoelectricity Technology Co., Ltd., Hangzhou 310018, China
[5] Center for Excellence in Nanoscience, Key Laboratory of Nanosystem and Hierarchical Fabrication, National Center for Nanoscience and Technology, Beijing 100190, P. R. China

1 Introduction

Organic–inorganic lead halide perovskite solar cells (PSCs) emerge as the next generation photovoltaic devices with the increasing demands for the renewable energy sources [1–6]. For planar PSCs, n-type and p-type semiconductors are arranged separately on both sides of perovskite active layer to transport electrons and holes [7, 8]. As a crucial part of the state-of-the-art PSCs, hole transport layer (HTL), is supposed to extract and transport photogenerated holes and block electrons efficiently [9]. Therefore, various basic requirements must be met when a hole transport material (HTM) is applied in PSCs, such as solubility, suitable energy level, and high hole mobility [10]. For the PSCs with typical n-i-p structure, 2,2′,7,7′-tetrakis(*N,N*-di-*p*-methoxy-phenylamine)-9,9′-spirobifluorene (Spiro-OMeTAD) is mostly utilized in high-efficiency PSCs [11]. However, it still suffers from some deadly disadvantages. For example, the poor

thermal stability and moisture tolerance come up after doping lithium bistrifluoromethane-sulfonimidate (Li-TFSI) and 4-tert-butylpyridine (tBP), which is originally aimed to overcome intrinsic low hole mobility [12]. Meanwhile, complicated synthesis and purification procedure will be a burden for fabrication and cost. So as to improve the photovoltaic performance and stability of PSCs, finding substitutions for Spiro-OMeTAD is of great importance. A variety of HTMs such as polymers, small molecules, and p-type inorganic materials are investigated [13]. Among them, organic small molecules are designed and used in PSCs owing to their advantages of structural diversity, high purity, and good repeatability. Except for the core of Spiro, the following building units, such as spiro(fluorene-9,9′-xanthene) (SFX), triphenylamine (TPA), tetraphenylethene, *N,N*′-bicarbazole, and triazines are used widely as the core of HTMs for outstanding performance [14–17]. However, the synthesis and purification of most of them is also complicated and consists of several steps.

SFX is an attractive core unit due to the easy synthesis procedures [18]. Several research groups have reported the SFX-based small-molecule HTMs used for PSCs with excellent PCEs [19, 20]. Derong Cao et al. reported a series of HTMs based on SFX and systematically investigated the structure–function relationship of the different donor units like methoxydiphenylamine-substituted carbazole and methoxydiphenylamine-substituted diphenylamine [21]. Sang Il Seok et al. synthesized SFX derivative with end-cap unit of *N*3, *N*6-bis(di-4-anisylamino)-9*H*-carbazole and finally obtained optimal PCE over 20% by using a quite lower concentration (28.57 mg/mL) than Spiro-OMeTAD [22]. When it comes to end-cap units, researches have confirmed that the stability of PSCs will be improved with the incorporation of F atoms [23]. Moreover, the substitution of fluorine could adjust the optical and electrical properties as well. Jinwei Gao et al. found that the introduction of F atom made HTM more hydrophobic and endowed the corresponding PSCs with better ambient stability [24]. Hence, trifluoroethoxy group ($-OCH_2CF_3$) is expected to further reduce the highest occupied molecular orbital (HOMO) energy level by the employment of strong electronegative F and enhance the long-term stability for a hydrophobic film [25, 26].

As the fundamental rule about energy alignment, HOMO and lowest occupied molecular orbital (LUMO) of HTMs should be slightly higher than the valence band maximum and conduction band minimum of perovskite layer. Then, the HTM could transfer holes and block electrons between perovskite layer and HTL in PSCs efficiently. In addition, when using different HTMs for fabricating a PSC, HOMO energy level will affect

the final open-circuit voltage (V_{OC}) [27–29]. In view of Shockley-Queisser limit, there is still room for further improvements in V_{OC}, along with better performance in efficiency. Therefore, for HTMs designer, energy alignment is supposed to be taken into consideration. The high HOMO energy level of HTMs brings out large energy offsets, which will become an interfacial obstacle for hole extraction and thus resulting in severe V_{OC} loss in PSCs [30]. Emilio Palomares et al. systematically investigated the influence of HTMs on the V_{OC} in depth and found that it is of great significance to tune the energetics at the interface between the HTL and the perovskite layer, such as the use of a self-assembled monolayer of molecular dipoles [27]. Abdi-Jalebi et al. showed significant enhancement in the charge extraction efficiency via energy alignment of HTL utilizing graded doping approach which in turn enhance both stability and efficiency of PSCs [31]. Therefore, selecting HTMs with suitable energy level is not only an excellent strategy to minimize the V_{OC} loss and enhance the V_{OC} for PSC, but also a facile method to promote the charge extraction and transport.

Herein, we report a new hole transport molecule with SFX core as a promising HTM for n-i-p PSCs, in which trifluoroethoxy group is used as the end-cap unit. A fine-tuned HOMO level is obtained in an effort to enhance the V_{OC}. Then, the impacts of better energy alignment between perovskite layer and HTL are investigated, and the change on V_{OC} is discussed. The champion device with SFX-POCCF3 as HTM shows a PCE of 21.48% with V_{OC} of 1.16 V. Furthermore, the device with SFX-POCCF3 retains 95% of the initial efficiency after about 1,000 h continuous light soaking at 25 °C, whereas the device with Spiro-OMeTAD degrades rapidly to 90% of its original PCE after 50 h. Overall, we offer a potential HTM for the enhancement of V_{OC} and efficiency in PSC devices. This work makes a highlight of advantages of the low HOMO level materials for the energy alignment and reduced voltage loss.

2 Results and discussions
2.1 Material characteristics

The synthetic routes and chemical structure for SFX-POCCF3 are shown in Fig. 1(a). And the detailed procedures are given in Supplementary document. ^{1}HNMR, ^{13}CNMR, and mass spectrometry were used for the identification of the synthesized compounds (Figs. S2, S3, S4 and S5). As we know, the high synthetic cost for Spiro-OMeTAD hinders its large-scale production. Thus, the cost for SFX-POCCF3 synthesis is calculated to quite low (23.72 $/g) in Table S1. Compared with the commonly used spirobifluorene (SBF) core in Spiro-OMeTAD, SFX-POCCF3 consists of an orthometric

Luo *et al. Carbon Neutrality*   (2023) 2:21

Page 3 of 9
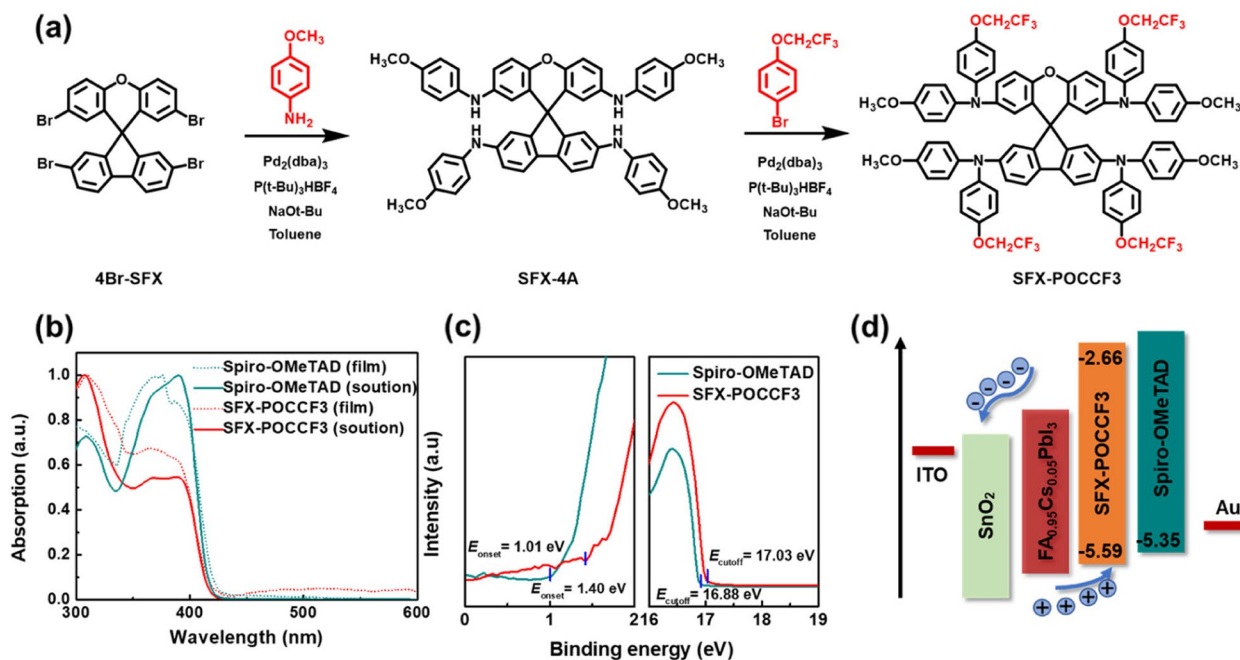
Fig. 1 (**a**) Synthetic route for SFX-POCCF3; (**b**) UV–Vis absorption spectra and (**c**) UPS spectra for SFX-POCCF3; (**d**) illustration for energy alignment

spiro-[fluorene-9,9′-xanthene] (SFX) unit as core and the additional oxygen atom in conjugated bridge can slightly reduce the planarity and the symmetry, leading to great effects on electrical and optical properties of HTM [32]. The synthesis of spiro-type SFX core (spiro[fluorene-9,9'-xanthene]) only needs one-pot route and can be purified by simple recrystallization along with high yield, which greatly reduced the cost. And the cost of SFX core (about 1.12 $/g) is 30 times lower than that of the spiro core (about 33.89 $/g), which were studied and compared in reported works of literature [19]. In our design strategy, the non-conjugated alkoxy chain trifluoroethoxy was introduced as the end-cap unit and it is expected to reduce the HOMO level and enhance the moisture endurance.

The geometric structure of SFX-POCCF3 is presented in Fig. S6, and the HOMO is also calculated by density functional theory (DFT), which brings a deep insight into the geometrical configuration and the electronic structure of SFX-POCCF3. Usually, twisty configuration endows the HTM good solubility and film-forming property, that is important for the solution manufacture

[32]. Similar with the SBF core unit, SFX core is twisted as well with a dihedral angles of 94.6°, leading to a good solubility in the common organic solvents. Moreover, the dopants are supposed to be added necessarily to enhance the hole mobility and conductivity for the loose packing caused by the twisty configuration. As shown in Fig. S6(b-c), it can be found that the HOMO of SFX-POCCF3 was mainly localized peripheral TPA arms with some extended to the core and the LUMO mainly localized toward the SFX core. And the HOMO and LUMO levels of SFX-POCCF3 are − 4.63 and − 1.07 eV by simulated calculation.

The optical properties of the investigated molecules were studied by UV–Vis absorption in chlorobenzene solution and thin films as illustrated in Fig. 1(b) and the corresponding data was listed in Table 1. In chlorobenzene solution, both of Spiro-OMeTAD and SFX-POCCF3 contain two absorption bands in the UV region. First, SFX-POCCF3 exhibits a wide absorption band from 350 to 400 nm representing π-π* transition of conjugated system [33]. While Spiro-OMeTAD shows a maximum absorption peak at 390 nm with a shoulder at 372

Table 1 Optical, electrochemical, and thermal properties of SFX-POCCF3 and Spiro-OMeTAD

HTM	λ_{onset} (nm)	E_g (eV)	E_{ox} (eV)	HOMO (eV)	LUMO (eV)	μ_h (cm^2 V^{-1} S^{-1})	T_d (℃)	T_g (℃)
SFX-POCCF3	423	2.93	0.875	−5.215	−2.285	3.11×10^{-4}	385	130
Spiro-OMeTAD	432	2.87	0.805	−5.137	−2.267	1.46×10^{-4}	422	126

Luo *et al. Carbon Neutrality*   (2023) 2:21

Page 4 of 9

nm. The second peaks appear 310 nm both for Spiro-OMeTAD and SFX-POCCF3, relating to the n-π* transition of TPA arms [34]. When in the film state, there is no obvious shift in SFX-POCCF3 spectrum for the maximum absorption and the intensity of absorption increases due to the enhanced intermolecular charge transfer [35]. The optical band gap (E_g) was calculated to be 2.93 eV and 2.87 eV by the equation of $E_g = 1240/\lambda_{onset}$, according to the edge of absorption spectra.

The thermal properties of SFX-POCCF3 were evaluated by thermogravimetric analysis (TGA) and differential scanning calorimetry (DSC) analysis. As shown in Fig. S7(a), this HTM possesses a high decomposition temperature (T_d, 5% weight loss) at 385 ℃. And the DSC trace demonstrates that it is amorphous and the glass transition temperatures (T_g) is 130.3 ℃. Compared with SFX-POCCF3, the T_d and T_g of Spiro-OMeTAD were tested to 422 and 126 ℃, respectively.

Generally, it is crucial for PSCs to get a well-matched energy level between perovskite layer and HTL. To investigated the electrical properties, the HOMO level of SFX-POCCF3 was first measured by a cyclic voltammetry (CV) measurement. The CV curves can be found in Fig. S8 and the data was listed in Table 1 as well. The oxidation onset (E_{ox}) of SFX-POCCF3 was 0.875 eV, which correspond to HOMO energy level of −5.215 eV (E_{HOMO} is obtained by the equation: $E_{HOMO} = 4.8 − E_{ox} − E_{Fe/Fe+}$). And the LUMO level can be obtained by E_{HOMO} and E_g from UV–Vis absorption spectra. Meanwhile, the HOMO of Spiro-OMeTAD was 5.137 eV, lower than that of SFX-POCCF3. In terms of the obtained HOMO and LUMO results, it can be assumed that the HOMO level of SFX-POCCF3 is deep enough to exact holes and the LUMO level makes sure successful electrons blocking from active layer. More importantly, the deeper HOMO level of SFX-POCCF3 contributes to the better energy alignment between perovskite layer and HTL, promoting charge transport and minimizing the V_{OC} loss.

Moreover, the HOMO and LUMO levels were tested in Fig. 1(c) by ultraviolet photoelectron spectroscopy (UPS) in film state as HTL onto the perovskite layer. The HOMO level can be calculated by the following equation: $E_{HOMO} = 21.22 − E_{cutoff} + E_{onset}$. As shown in Fig. 1(c), the HOMO level of SFX-POCCF3 was −5.59 eV and LUMO level was calculated to be −2.66 eV, lower than that of Spiro-OMeTAD, which is consistent with the CV results.

Hole mobility (μ_h) of those HTMs is tested by space-charge-limited current (SCLC) method with structure of ITO/PEDOT:PSS/HTM/MoO₃/Al. In general, low hole mobility and conductivity are the common drawbacks for HTM with twisted structure. In contrast to SBF unit, when oxygen atom is introduced into conjugated bridge, the planarity and the symmetry of SFX will be reduced.

As results in Fig. S9, the hole mobility of SFX-POCCF3 is calculated to be 3.11×10^{-4} cm² V⁻¹ s⁻¹, that is more than two times higher than that of Spiro-OMeTAD (1.46×10^{-4} cm² V⁻¹ s⁻¹).

2.2 Device performances

Firstly, to assess the photovoltaic performance of HTM, SFX-POCCF3 was introduced into the PSCs acting as HTL with a commonly used n-i-p structure. The illustration of charge extraction processes was given in Fig. 1(d). Compared with Spiro-OMeTAD, SFX-POCCF3 possesses a deeper HOMO level, which is beneficial for charge extraction and transfer due to the lower barrier to overcome.

To make a comparison, SFX-POCCF3 was utilized as HTM in PSC with the Spiro-OMeTAD based device as control. The film morphology of these HTMs deposited on perovskite was studied by scanning electron microscopy (SEM) and atomic force microscopy (AFM) measurements, respectively. The top-view SEM images are shown in Fig. 2(a-c), the HTM-covered films turn into indistinct due to the electron-blocking effect. The cross-section view SEM images of devices based on different HTMs were shown in Fig. 2(d-f). Compared with ultrathin undoped HTM films, the thickness of SFX-POCCF3 is around 130 nm, which is thinner than that of the thickness of Spiro-OMeTAD (180 nm). As for as concerned, sufficient thickness for HTL should be considered for the effective electrons blocking. And the thickness of HTL is determined by the concentration and spin-coating rate. As illustrated in Fig. 2(g-i), when Spiro-OMeTAD and SFX-POCCF3 were spin-coated onto the perovskite film, the root-mean-square (RMS) roughness reduced to 7.78 and 8.56 nm, respectively. For undoped SFX-POCCF3 HTMs, the RMS was 11.79 nm. All these results confirm a good surface coverage without pinholes for HTM films, which facilitate the charge transfer. Furthermore, photoluminescence is used to test the charge extraction and transfer processes. As exhibited in Fig. S10, pure perovskite film showed a high peak at 802 nm. Once HTM was deposit onto the perovskite, PL intensity witnessed a sharp decrease, indicating the quenching effect from HTM. In comparison with Spiro-OMeTAD, a more efficient quenching was observed related to SFX-POCCF3, suggesting better hole extraction by SFX-POCCF3 and better charge transfer between HTL and perovskite layer.

To estimate the photovoltaic performance, we firstly investigated the concentration of SFX-POCCF3 on the device performance. The *J-V* curves of different concentration of SFX-POCCF3 are posted on the Fig. S11(a) and the corresponding photovoltaic parameters are listed in Table S2. The PSC fabricated with 70 mg/mL possessed a relative lower V_{OC} and J_{SC} of 1.11 V and 23.92 mA cm⁻²,

Luo *et al. Carbon Neutrality*   (2023) 2:21

Page 5 of 9
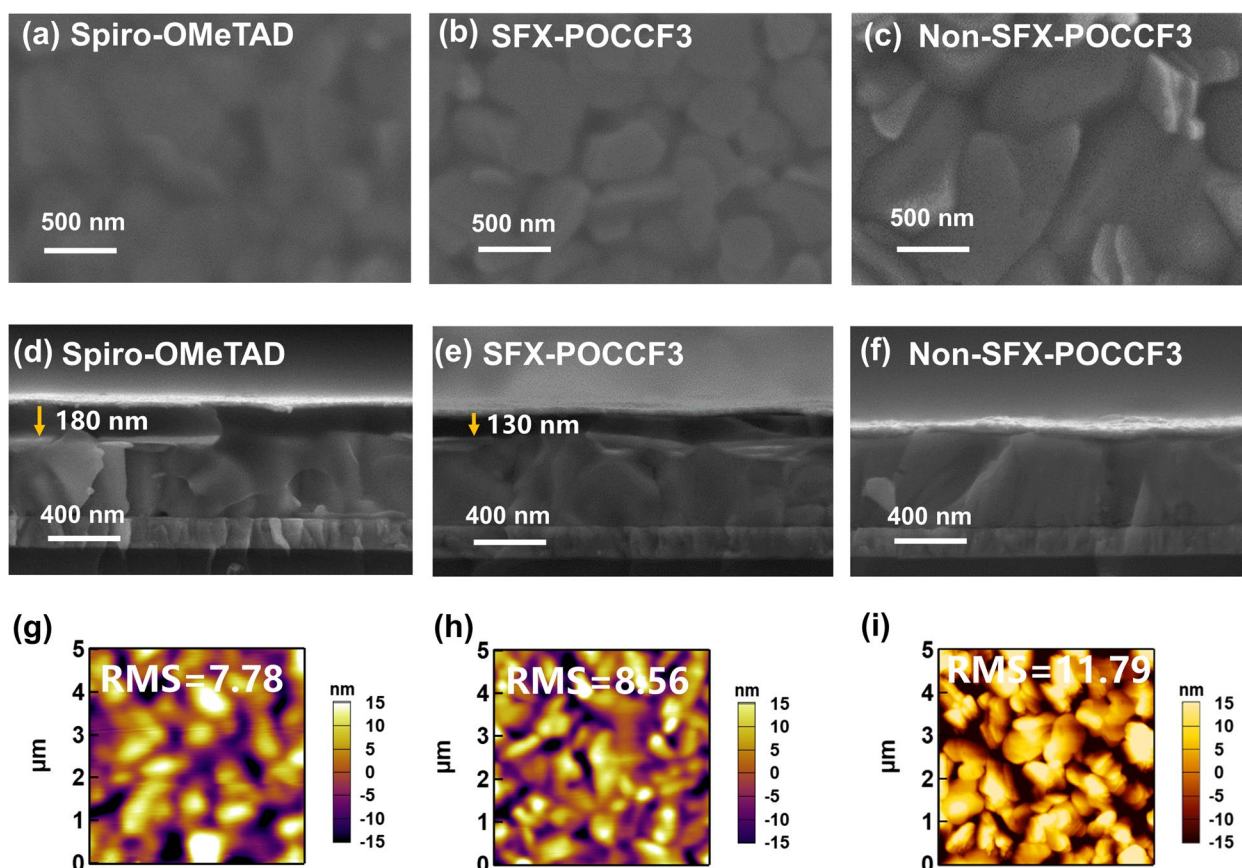
Fig. 2 Top-view SEM images of Spiro-OMeTAD film (**a**), SFX-POCCF3 film (**b**), undoped SFX-POCCF3 film, and (**c**) spin-coated on perovskite layer; Cross-sectional SEM images of devices based on Spiro-OMeTAD (**d**), SFX-POCCF3 (**e**), and undoped SFX-POCCF3 film (**f**); Top-view AFM topographical images of Spiro-OMeTAD film (**g**), SFX-POCCF3 film (**h**), and undoped SFX-POCCF3 film (**i**) spin-coated on perovskite layer

thus leading to a poor PCE of 18.90%. When the concentration increases to 80 mg/mL, it showed a remarkable increase on V_{OC} (1.13 V). Finally, a concentration of 90 mg/mL exhibited an outstanding performance of 20.58% in the same test batch. An increase on V_{OC} (30 mV) is observed, which is attributed to that HTL is thick enough to block electrons effectively and suppress the recombination between holes and electrons. The spin-coating rate was studied at the optimal concentration of 90 mg/mL and the rate of 6000 rpm was confirmed to be best in Fig. S11(b) and Table S3. Last but not least, the influences of different amounts of additives like Li-TFSI and tBP were investigated in Fig. S12. For the tests of adding amount of Li-TFSI, the volume of tBP was fixed to be 36 μL/mL. And the volume of tBP was adjusted with a fixed amount of Li-TFSI of 22 μL/mL in turn. It is clear that without additives or a small amount of them, the devices showed very low PCEs. That is mainly ascribed to the poor conductivity and hole mobility, which cannot ensure holes transported successfully to the electrode. As results, there is a reduction on FF and J_{SC}.

When the amount of Li-TFSI increase over 36 μL/mL, the PCEs presented sharp decreases, together with the abruptly drops on V_{OC} and FF. This decrease is caused by the insoluble complexes of Li-TFSI reacting with HTMs, leading to poor film morphology out of flatness and hindering the carrier migration.

Eventually, the *J-V* curves of champion devices with optical concentration, spin-coating rate and doping amount are presented in Fig. 3(a) under forward scanning directions. And the detailed statistics are listed in Table 2 and Fig. S14. The champion device with SFX-POCCF3 presented a high PCE of 21.48% (V_{OC} = 1.16 V, FF = 75.60%, J_{SC} = 24.56 mA cm^{-2}), higher than the champion PCE of control device (21.39%), suggesting better performance on the photovoltaic properties. In addition, the statistical distributions under reverse scanning direction of the PCE, FF, V_{OC}, J_{SC} are displayed in Fig. 3(b) and Fig. S14 to prove the good reproducibility, the corresponding parameters are summarized in Table 2 as well. It is clear to see that SFX-POCCF3 possessed higher V_{OC} and J_{SC}, along with slightly decreased FF. The

Luo *et al. Carbon Neutrality*   (2023) 2:21

Page 6 of 9
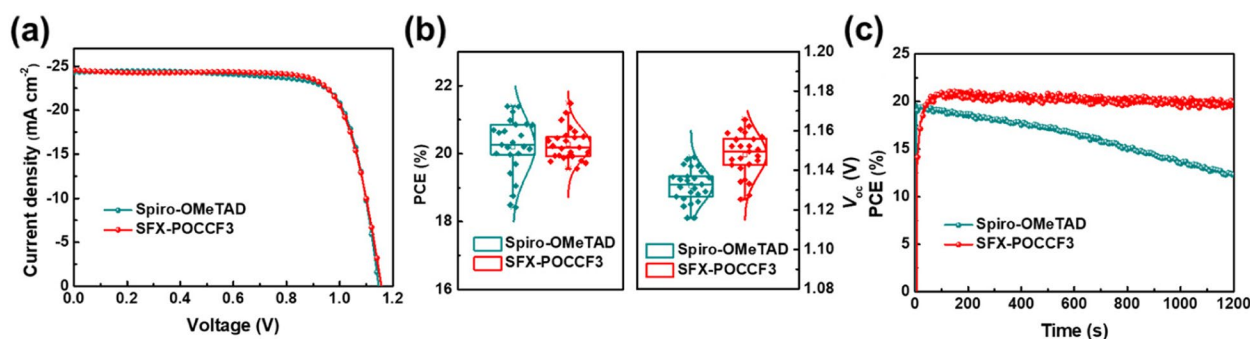
Fig. 3 (**a**) *J-V* curves of champion PSC devices based on different HTMs under reverse scanning directions; statistics of PCE and V_{OC} (**b**) from 25 individual devices; (**c**) Steady-state photocurrent and PCE of the devices under a voltage bias at the maxima power point

Table 2 Photovoltaic performance parameters of champion devices and average parameters of the 25 devices

HTM	Direction	V_{OC} (V)	FF (%)	J_{SC} (mA cm^{-2})	PCE (%)
Spiro-OMeTAD	Forward	1.13	70.83	24.59	19.78
	Reverse	1.14	76.73	24.32	21.39
	Average	1.13 ± 0.01	73.42 ± 2.86	24.30 ± 0.40	20.20 ± 0.84
SFX-POCCF3	Forward	1.15	64.44	24.98	18.46
	Reverse	1.16	75.60	24.56	21.48
	Average	1.15 ± 0.01	72.29 ± 1.74	24.43 ± 0.34	20.27 ± 0.48

improvement of V_{OC} and J_{SC} is attributed to better energy alignment, shortening the carrier transport path. As we know, a solar cell can also act as a light emitting diode (LED) when bias applied. Calculated by the following equation: $\Delta V_{OC}^{nonrad} = -\frac{K_B T}{q} ln EQE_{EL}$, where K_B is Boltzmann's constant, T is temperature. ΔV_{OC}^{nonrad} is obtained to evaluate non-radiative recombination process when injection current is equal to photocurrent of solar cell device. In Fig. S15(a), SFX-POCCF3 reached a EQE_{EL} of 3.85% at 1.82 V, as Spiro-OMeTAD only achieved 1.85% at 1.62 V, which is in accordance with the improvement of V_{oc} for PSC. From Fig. S15(b), when the injection current is similar with photocurrent, SFX-POCCF3 and Spiro-OMeTAD devices can got 1.80% and 0.98%. Thus, the nonradiative recombination voltage loss ΔV_{OC}^{nonrad} is 103 mV and 119 mV, respectively. The stabilized PCE and current density at maximum power point are shown in Fig. 3(d). Clearly, the PCE of Spiro-OMeTAD device decreased sharply from 19.61% to 12.29%, indicating a poor photo stability. The device with SFX-POCCF3 exhibited an outstanding stabilized efficiency during 1200 s and the average PCE is stabilized at 20.66% with relevant J_{SC} of 23.03 mA cm^{-2}. For the undoped devices, they display similar trend for the continuous output with PCE around 17.5%.

Multiple factors, including ion migrations, intrinsic defects and lattice strain release have been proved to have significant effect on device stability [36, 37]. To access the light stability, the devices were put in the argon glove box without encapsulation and a LED light was applied to imitate the sun light. The SFX-POCCF3 showed a superior stability under the continuous illumination with negligible degradation after 800 h in Fig. 4(a). Whereas the control device degraded rapidly for only 90% of its original PCE after 100 h and showed an obvious fluctuation. The X-ray diffraction (XRD) tests were used to value the degradation process when the devices were put in the natural environment indoor with sub rise and sun set (relative humidity: 30–40%). After exposure to the light for 10 days, the device based on Spiro-OMeTAD exhibited higher PbI$_2$ peak than that of SFX-POCCF3, which is in correspondence with the stability test results. To illustrate the factor regarding stability, contact angle was conducted to test the waterproof ability. SFX-POCCF3 displayed a higher contact angle of 87.43°, whereas Spiro-OMeTAD only showed 62.62° in Fig. S16. It is indicated that devices based SFX-POCCF3 will have better tolerance in the humid environment. We further conducted stability test based on the unencapsulated device in ambient environment with humidity around 30–40%. In Fig. S16(b), SFX-POCCF3 device can maintain over 85% of starting efficiency after 500 h. The changes of thin film samples are recorded in Fig. S16(d), it is obvious that
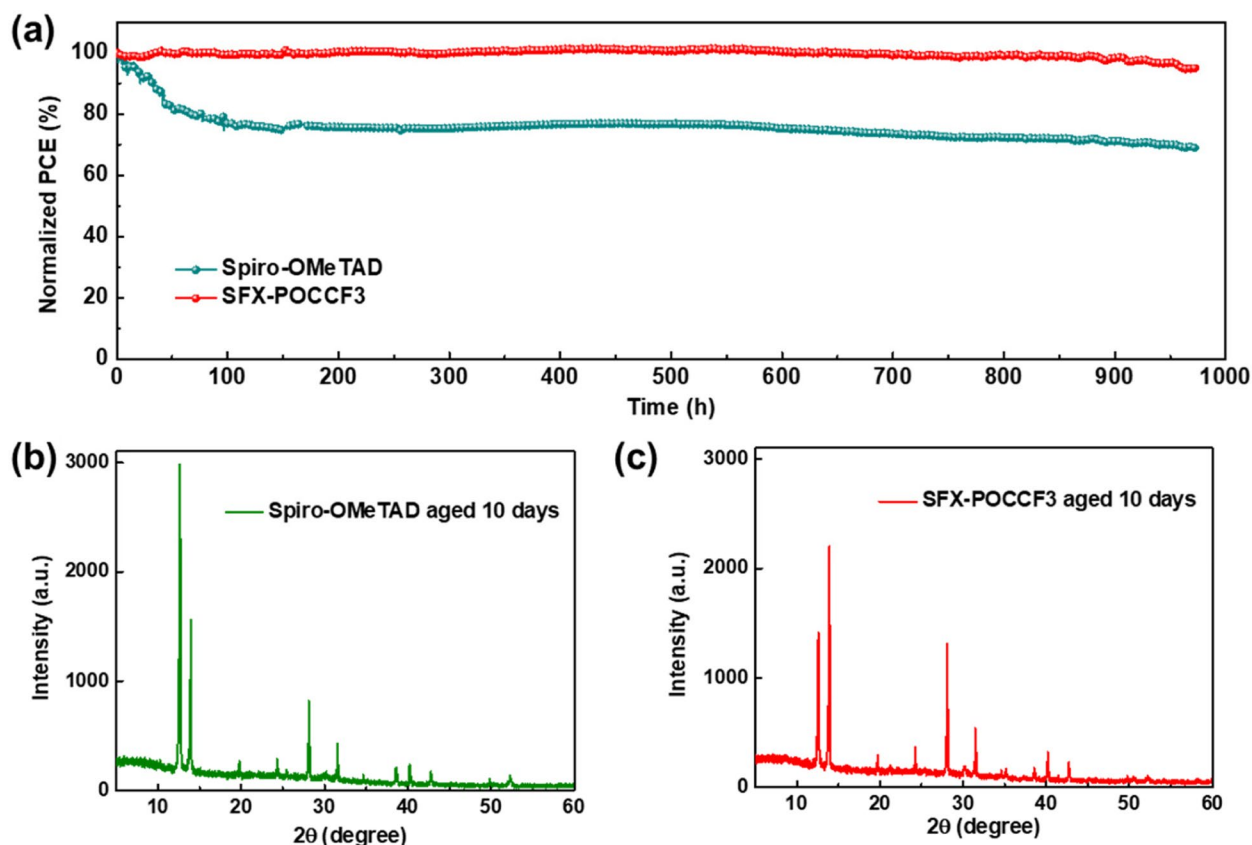
Fig. 4 (**a**) Stability of unencapsulated devices under the continuous illumination; XRD spectra for (**b**) Spiro-OMeTAD and (**c**) SFX-POCCF3 based devices after continuous light exposure for 10 days

yellow phase PbI_2 appears on Spiro-OMeTAD sample after 7days' aging, indicating water induced phase segregation [38, 39].

3 Conclusions

In summary, a new hole transport material (SFX-POCCF3) is synthesized as the substitute for commonly used Spiro-OMeTAD. First, low-cost SFX is applied as the core unit and the oxygen bridge can improve the solubility. Second, for the terminal group, F atoms are considered to modulate the energy level of the molecule. As a result, SFX-POCCF3 showed a low HOMO level, thus leading to the higher V_{OC} in PSCs with a champion PCE of 21.48%. More importantly, the unencapsulated cells showed super light duration, which retained 95% of the initial efficiency after about 1,000 h continuous light soaking. This work demonstrated the great promise of that suitable energy level of SFX-POCCF3 for accessing high-performance PSCs.

Abbreviations
PSC   Perovskite solar cell

SFX	Spiro[fluorene-9,9'-xanthene]
HTM	Hole transport material
HTL	Hole transport layer
LiTFSI	Lithium bistrifluoromethane-sulfonimidate
tBP	4-Tert-butylpyridine
TPA	Triphenylamine
HOMO	Highest occupied molecular orbital
LUMO	Lowest occupied molecular orbital
SBF	Spirobifluorene
DFT	Density functional theory
TGA	Thermogravimetric analysis
DSC	Differential scanning calorimetry
E_g	Band gap
CV	Cyclic voltammetry
UPS	Ultraviolet photoelectron spectroscopy
SCLC	Space-charge-limited current
SEM	Scanning electron microscopy
AFM	Atomic force microscopy
RMS	Root-mean-square
XRD	X-ray diffraction

Supplementary Information

The online version contains supplementary material available at https://doi.org/10.1007/s43979-023-00061-9.

Additional file 1: Fig. S1. Synthetic route of SFX-POCCF3. **Fig. S2.** ^{1}H NMR spectrum of SFX-4A. **Fig. S3.** The ^{1}H NMR spectrum of SFX-POCCF3. **Fig. S4.** The ^{13}C NMR spectrum of SFX-POCCF3. **Fig. S5.** The MALDI-TOF-MS spectrum of SFX-POCCF3. **Fig. S6.** (a) Geometric structure of

Luo *et al. Carbon Neutrality*   (2023) 2:21

Page 8 of 9

SFX-POCCF3; HOMO (b) and LUMO (c) distributions of SFX-POCCF3. **Fig. S7.** (a) Thermogravimetric and (b) Differential scanning calorimetry curves of SFX-POCCF3 measured under a nitrogen atmosphere. **Fig. S8.** CV curves of the Spiro-OMeTAD and SFX-POCCF3 HTMs. **Fig. S9.** Hole mobility of Spiro-OMeTAD and SFX-POCCF3. **Fig. S10.** Photoluminescence spectra of perovskite thin film with or without hole transport material covering. **Fig. S11.** (a) *J-V* curves of PSCs fabricated using various concentrations of SFX-POCCF3 in the same batch. (b) *J-V* curves of PSCs fabricated with different spin-coating rates of SFX-POCCF3 in the same batch. **Fig. S12.** Relationship between PCE and the amounts of dopants added to SFX-POCCF3 solution. The added volume of Li-TFSI means the amount of Li-TFSI solution in acetonitrile (540 mg mL^{-1}). **Fig. S13.** The *J-V* curves of champion devices from the forward and reverse direction. **Fig. S14.** Statistics of FF (a) and J_{SC} (b) from 25 individual devices. **Fig. S15.** (a) Best EQE electroluminescence as a function of voltage of PSCs operating as LEDs. Inset: EL image when PSC act as an LED displays a clearly visible red emission under ambient light. **Fig. S16.** Contact angles of (a) Spiro-OMeTAD and (b) SFX-POCCF3. (c) humidity stability of devices; (d) Images of fresh Spiro-OMeTAD and SFX-POCCF3 on top of perovskite film, after putting in ambient air for 7 days. **Table S1.** The cost of SFX-POCCF3 product. **Table S2.** Photovoltaic performance parameters of PSCs fabricated using various concentrations of SFX-POCCF3 in the same batch. **Table S3.** Photovoltaic performance parameters of PSCs fabricated using different spin-coating rates of SFX-POCCF3 in the same batch. **Table S4.** Photovoltaic performance parameters of PSCs fabricated using different adding amount of Li-TFSI in the same batch. **Table S5.** Photovoltaic performance parameters of PSCs fabricated using different adding amount of tBP in the same batch.

Acknowledgements

Authors' contributions
HL and ZZ contributed equally to this work. KY and KG conceived the idea and supervised the overall project. HL designed the experiments. ZZ synthesized the HTM. LY and JW helped on the device fabrication and characterization. BL and SW characterized the structure of HTM and performed DTF calculations. MA and LD reviewed the manuscript. The final version of the paper has been approved by all authors.

Funding

Availability of data and materials
The data and materials are available upon reasonable request.

Declarations

Ethics approval and consent to participate
All co-authors certify that the submission is original unpublished work and is not uder review elsewhere.

Consent for publication
All authors agree to the publication of this manuscript.

Competing interests
The authors declare that they have no known competing financial interests or personal relationships that could have appeared to influence the work reported in this paper.

References
1. Matthew DS, Bridget AC, Hemamala IK (2019) Tuning the luminescence of layered halide perovskites. Chem Rev 119:3104–3139. https://doi.org/10.1021/acs.chemrev.8b00477
2. Zhi-Kuang T, Reza Saberi M, May Ling L et al (2014) Bright light-emitting diodes based on organometal halide perovskite. Nat Nanotechnol 9:687–692. https://doi.org/10.1038/nnano.2014.149
3. Letian D, Yang (Micheal) Y, Jingbi Y et al (2014) Solution-processed hybrid perovskite photodetectors with high detectivity. Nat Commun 5:5404. https://doi.org/10.1038/ncomms6404
4. Akihiro K, Kenjiro T, Yasuo S, Tsutomu M (2009) Organometal halide perovskites as visible-light sensitizers for photovoltaic cells. J Am Chem Soc 131:6050–6051. https://doi.org/10.1021/ja809598r
5. NREL National Renewable Energy Laboratory. NREL Efficiency Chart. https://www.nrel.gov/pv/cell-efficiency.html (Accessed on 1 Jan 2023)
6. Yang S, Kong-Chao S, Yan-Qing L et al (2021) Interfacial potassium-guided grain growth for efficient deep-blue perovskite light-emitting diodes. Adv Funct Mater 31:2006736. https://doi.org/10.1002/adfm.202006736
7. Shengfan W, Zhen L, Mu-Qing L et al (2020) 2D metal-organic framework for stable perovskite solar cells with minimized lead leakage. Nat Nanotechnol 15:934–940. https://doi.org/10.1038/s41565-020-0765-7
8. Fei Z, Kai Z (2019) Additive engineering for efficient and stable perovskite solar cells. Adv Energy Mater 10:1902579. https://doi.org/10.1002/aenm.201902579
9. Sureshraju V, Weijun K, Pragya P et al (2019) Benzodithiophene hole-transporting materials for efficient tin-based perovskite solar cells. Adv Funct Mater 29:1905393. https://doi.org/10.1002/adfm.201905393
10. Guan-Woo K, Hyuntae C, Minjun K et al (2020) Hole transport materials in conventional structural (n-i-p) perovskite solar cells: from past to the future. Adv Energy Mater 10:1903403. https://doi.org/10.1002/aenm.201903403
11. Jin Young K, Jin-Wook L, Hyun Suk J, Hyunjung S, Nam-Gyu P (2020) High-efficiency perovskite solar cells. Chem Rev 120:7867–7918. https://doi.org/10.1021/acs.chemrev.0c00107
12. Xiaoming Z, Chao Y, Kaichen G, Tianran L, Yu X, Yueh-Lin L (2020) A hole-transport material that also passivates perovskite surface defects for solar cells with improved efficiency and stability. Energy Environ Sci 13:4334–4343. https://doi.org/10.1039/D0EE01655A
13. Jiangzhao C, Ja-Young S, Nam-Gyu P (2018) Simultaneous Improvement of Photovoltaic Performance and Stability by In-situ Formation of 2D Perovskite at (FAPbI3)$_{0.88}$(CsPbBr3)$_{0.12}$/CuSCN Interface. Adv Energy Mater 8:1702714. https://doi.org/10.1002/aenm.201702714
14. Xiang-Dong Z, Xing-Juan M, Ya-Kun W et al (2019) Hole-transporting materials incorporating carbazole into spiro-core for highly efficient perovskite solar cells. Adv Funct Mater 29:1807094. https://doi.org/10.1002/adfm.201807094
15. Sadia A, Malik AR, Samia AK et al (2016) Perovskite solar cells: influence of hole transporting materials on power conversion efficiency. ChemSusChem 9:10–27. https://doi.org/10.1002/cssc.201501228
16. Laura C, Samrana K, Michael G, Shahzada A (2016) Hole-transport materials for perovskite solar cells. Angew Chem Int Ed 55:14522–14545. https://doi.org/10.1002/anie.201601757
17. Weiqi Z, Zhenhai W, Peng G (2018) Less is more: dopant-free hole transporting materials for high-efficiency perovskite solar cells. Adv Energy Mater 8:1600502. https://doi.org/10.1002/aenm.201702512
18. Michal M, Aruna I, Neil R (2016) SFX as a low-cost 'Spiro' hole-transport material for efficient perovskite solar cells. J Mater Chem A 4:4855–4863. https://doi.org/10.1039/C6TA00110F

Luo *et al. Carbon Neutrality*   (2023) 2:21

Page 9 of 9

19. Dongqin B, Bo X, Peng G, Licheng S, Michael G, Anders H (2016) Facile synthesized organic hole transporting material for perovskite solar cell with efficiency of 19.8%. Nano Energy 23:138–144. https://doi.org/10.1016/j.nanoen.2016.03.020

20. Sivakumar G, Rajneesh M (2018) Spiro-linked organic small molecules as hole-transport materials for perovskite solar cells. J Mater Chem A 6:18750–18765. https://doi.org/10.1039/C8TA08503J

21. Yajie F, Yang L, Qingliang Z, Hanlun W, Lingyun W, Hao T, Guichuan X, Derong C (2016) Influence of Donor Units on Spiro[fluorene-9,9′-xanthene]-based Dopant-free Hole-Transporting Materials for Perovskite Solar Cells. Sol Energy 216:180–187. https://doi.org/10.1016/j.solener.2021.01.004

22. Do YL, Gangala S, Manju RM, Sang IS (2020) Carbazole-Based Spiro[fluorene-9,9′-xanthene] as an efficient hole-transporting material for perovskite solar cells. ACS Appl Mater Interfaces 12:28246–28252. https://doi.org/10.1021/acsami.0c06318

23. Fangchao L, Jianyu Y, Xufeng L, Yannan Z et al (2018) A universal strategy to utilize polymeric semiconductors for perovskite solar cells with enhanced efficiency and longevity. Adv Funct Mater 28:1706377. https://doi.org/10.1002/adfm.201706377

24. Xiangyu K, Yue J, Xiayan Wu et al (2020) Dopant-free F-substituted ben-zodithiophene copolymer hole-transporting materials for efficient and stable perovskite solar cells. J Mater Chem A 8:1858–1864. https://doi.org/10.1039/C9TA11744J

25. Bin L, Yuan C, Xia T et al (2021) Decorating hole transport material with CF_3 groups for highly efficient and stable perovskite solar cells. J Energy Chem 62:523–531. https://doi.org/10.1016/j.jechem.2021.04.017

26. Zheng Z, Ligang Y, Bin L et al (2021) A Trifluoroethoxyl functionalized spiro-based hole-transporting material for highly efficient and stable perovskite solar cells. Sol RRL 6:2100944. https://doi.org/10.1002/solr.202100944

27. Ilario G, Núria FM, Ana PR et al (2019) Energy alignment and recombina-tion in perovskite solar cells: weighted influence on the open circuit voltage. Energy Environ Sci 12:1309–1316. https://doi.org/10.1039/C9EE00528E

28. Naveen KE, Ashraf U (2016) Open circuit voltage of organic solar cells: an in-depth review. Energy Environ Sci 9:391–410. https://doi.org/10.1039/C5EE02871J

29. Jose MM, Luis L, Emilio P (2016) Decreasing charge losses in perovskite solar cells through mp-TiO_2/MAPI interface engineering. Chem Mater 28:207–213. https://doi.org/10.1021/acs.chemmater.5b03902

30. Li W, Wenxiao Z, Sheng F et al (2020) Achieving over 21% efficiency in inverted perovskite Ssolar cells by fluorinating a dopant-free hole trans-porting material. J Mater Chem A 8:6517–6523. https://doi.org/10.1039/D0TA00522C

31. Mojtaba A, Ibrahim Dar M et al (2019) Charge extraction via graded dop-ing of hole transport layers gives highly luminescent and stable metal halide perovskite devices. Sci Adv 5:eaav2012 https://www.science.org/doi/abs/10.1126/sciadv.aav2012

32. Weidong L, Fan L, Qianqian L, Zhen L (2021) The crucial roles of the configurations and electronic properties of organic hole-transporting molecules to the photovoltaic performance of perovskite solar cells. J Mater Chem A 9:18148–18163. https://doi.org/10.1039/D1TA03718H

33. Minh AT, Hayoon L, Ai S et al (2021) Near-ultraviolet transparent organic hole-transporting materials containing partially oxygen-bridged triph-enylamine skeletons for efficient perovskite solar cells. ACS Appl Mater Interfaces 4:1484–1495. https://doi.org/10.1021/acsaem.0c02677

34. Zhaoning L, Yikai Y, Hongyan H et al (2021) Fluorine substitution position effects on spiro(fluorene-9,9′-xanthene) cored hole transporting materi-als for high-performance planar perovskite solar cells. J Energy Chem 57:341–350. https://doi.org/10.1016/j.jechem.2020.08.041

35. Qi J, Zhenyi N, Guiying X et al (2020) Interfacial molecular doping of metal halide perovskites for highly efficient solar cells. Adv Mater 32:200158. https://doi.org/10.1002/adma.202001581

36. Bai Y et al (2022) Initializing film homogeneity to retard phase segrega-tion for stable perovskite solar cells. Science 378:747–754. https://doi.org/10.1126/science.abn3148

37. Wei X, Xiao M, Wang B et al (2022) Avoiding structural collapse to reduce lead leakage in perovskite photovoltaics. Angew Chem Int Ed 61:e202204314. https://doi.org/10.1002/anie.202204314

38. Li Z, Li B, Wu X et al (2022) Organometallic-functionalized interfaces for highly efficient inverted perovskite solar cells. Science 376:416–420. https://doi.org/10.1126/science.abm8566

39. Wang H, Liu H, Dong Z et al (2022) Extracting ammonium halides by solvent from the hybrid perovskites with various dimensions to promote the crystallization of $CsPbI_3$ perovskite. Nano Energy 94:106925. https://doi.org/10.1016/j.nanoen.2022.106925

Publisher's Note